Surface & Coatings Technology 231 (2013) 583–589

Contents lists available at ScienceDirect

Surface & Coatings Technology

journal homepage: www.elsevier.com/locate/surfcoat

A high packing density micro-thermoelectric power generator based on film thermoelectric materials fabricated by electrodeposition technology

Wei Wang [a,*], Yu Ji [a], Han Xu [a], Huan Li [a], T. Visan [b], F. Golgovici [b]

[a] School of Chemical Engineering and Technology, Tianjin University, Tianjin 300072, PR China
[b] Dept. of Applied Physical Chemistry & Electrochemistry, University Politehnica of Bucharest, Romania

ARTICLE INFO

Available online 21 April 2012

Keywords:
Electrodeposition
Thermoelectric films
Micro-thermoelectric power generator
Fabrication
Properties

ABSTRACT

N-type $Bi_2Te_{2.7}Se_{0.3}$ thermoelectric (TE) compound and p-type $Bi_{0.5}Sb_{1.5}Te_3$ TE compound have been synthesized by electrodeposition combined with annealing treatment. Their composition, structure and morphology are characterized by XRD, EDS and SEM. The performances of the deposited films were also measured. The as-deposited films possess amorphous structure and they can be transferred to nano-crystal after anneal treatment. The annealed films show a preferred orientation along (015) crystal plane. Anneal treatment can also improve the performance of the deposited films efficiently. A micro-thermoelectric power generator (MTEG) module with high packing density of film TE legs was proposed, in which the heat transfers along the surface direction of the TE legs. Based on the proposed module, a MTEG containing 160 film thermocouples was fabricated and its size was 4 mm (height) × 25 mm (width) × 1 mm (thickness). Its open-circuit voltage, maximum output power and corresponding power density under a temperature difference of 20 K at 25 °C are 660 mV, 77 μW and 770 μW cm^{-3}, respectively.

1. Introduction

Thermoelectric (TE) materials and thermoelectric power generators have attracted considerable interest recently due to the requirements for environmental protection and reproducible energy. Bismuth–telluride-based materials are still considered to be the most suitable TE materials used in thermoelectric devices near room temperature. The performance of TE materials is directly related to the dimensionless figure of merit, ZT($ZT = (\alpha^2/\kappa\rho)T$), where α is the Seebeck coefficient, ρ is the electrical resistivity, κ is the thermal conductivity, and T is the absolute temperature. In recent years, nano-materials have shown enhanced ZT due to the quantum effects in its structure [1–23]. Several techniques have been used to synthesize TE films, such as chemical vapor deposition (CVD) [7], molecular beam epitaxy (MBE) [8], vapor–liquid–solid growth [9], electrochemical atomic layer epitaxy [11] and electrodeposition [12–23]. Electrodeposition offers the advantages of simple, easy operation and low cost. Moreover, the doping concentration, crystalline state and film thickness of TE materials can be easily controlled by adjusting the composition of the solution and electrodeposition parameters.

Miniaturized solid-state devices such as MEMS, micro-electrical system and even "system on a chip" are of interest for a variety of space and terrestrial applications. For those micro-systems, micro-power sources with low power and high out-put voltage are necessary. Micro-thermoelectric power generators (noted as MTEG) based on film thermoelectric materials have been considered to be a very promising candidate [24–31]. Fleurial et al. [32] fabricated a MTEG contained 126 TE legs (60 μm in diameter and 20 μm in height). The temperature difference was set up along the thickness direction of the TE legs. The maximum output power was measured to be 1 μW. Whalen et al. [33] built and tested a prototype MTEG which consisted of 22 wagon wheel-shaped TE legs (11 thermocouples) fabricated from 215 μm thick bismuth–telluride wafers having ZT = 0.97 at 30 °C. The temperature difference was set up along the surface direction of the wheel-shaped thermocouples. A peak output power of 450 μW could be obtained under the load of 3.7 Ω and temperature difference ΔT = 15 °C, which corresponded to a power density of 104 μW cm^{-3}, current of 11 mA, voltage of 41 mV and efficiency of 0.3%.

In our lab, n-type $Bi_2Te_{2.7}Se_{0.3}$ compound and p-type $Bi_{0.5}Sb_{1.5}Te_3$ compound have been synthesized by electrodeposition combined with annealing treatment. Their composition, structure and morphology are characterized by XRD, EDS and SEM. The performances of the deposited films were also measured. In addition, a micro-thermoelectric power generator (MTEG) module [34] with high packing density of film TE legs was proposed, in which the heat transfers along the surface direction of the TE legs. Based on the proposed module, an MTEG including 160 film thermocouples was fabricated and its size was 4 mm (height) × 25 mm (width) × 1 mm (thickness). The results will be presented here.

2. Experiment

2.1. Preparation of n-type and p-type film TE materials

All the chemicals used in the experiment were of analytical grade, and the solutions were prepared using redistilled water to ensure the

* Corresponding author. Tel.: +86 22 27402895; fax: +86 22 27409483.
E-mail address: wwangg@tju.edu.cn (W. Wang).

0257-8972/$ – see front matter © 2012 Elsevier B.V. All rights reserved.
doi:10.1016/j.surfcoat.2012.04.048

Table 1
Compositions of the solutions.

Solutions	Bi^{3+}	$HTeO_2^+$	H_2SeO_3	Sb^{III}	HNO_3	KNO_3
Bi–Te–Sb	2 mM	10 mM	–	100 mM	1 M	100 g L^{-1}
Bi–Te–Se	8 mM	8 mM	1 mM	–	1 M	100 g L^{-1}

stability of the ions in the solutions. Two kinds of solutions named Bi–Te–Se solution and Bi–Te–Sb solution were used to deposit n-type and p-type film TE materials, separately. Their compositions are listed in Table 1.

A potentiodynamic scanning method was used to deposit n-type and p-type thermoelectric films. The potentiodynamic deposition process was conducted at a potential scanning range from 0.04 V to −0.1 V for depositing n-type TE film and from 0.0 V to −0.2 V for depositing p-type TE film, and the potential scanning rate was 20 mV/s. All the potentials were measured and expressed related to an aqueous KCl saturated calomel electrode (SCE). Annealing treatment of as-deposited films was conducted at 250 °C for 12 h under nitrogen atmosphere and the films were embedded in a special instrument to avoid the variation of the composition.

2.2. Electrochemical measurement

All the electrochemical measurements were performed using CHI660B electrochemical working station at 25 ± 1 °C. A standard three-electrode cell was used for the electrochemical measurement, which consists of a gold plate (1 cm × 1 cm) as the working electrode, a Pt plate as the auxiliary electrode and a saturated calomel electrode (SCE) as the reference electrode. The working electrode was mechanically polished, electrochemically degreased, etched in concentrated HNO_3 solution and rinsed with redistilled water in order to ensure a clean surface before the measurements. All the potentials were measured and expressed related to an aqueous KCl saturated calomel electrode (SCE). Voltammetry was conducted at a scanning rate of 20 mV/s.

2.3. Characterization of film n-type and p-type thermoelectric materials

The morphologies of the deposited films were analyzed using an environment scanning electron microscope (ESEM, PHILIPS XL30). The compositions of the deposited films were analyzed using an energy dispersive spectrometer (EDS) (XL30 ESEM TMP, Philips, UK). The X-ray diffraction (XRD) patterns of the deposited films were obtained with a film X-ray diffractometer (XRD) using CuKalpha radiation (Philips PANalytical X'pert MPD, 10 kV, 200 mA, scan rate 4°/min). The grain sizes were calculated by the Scherrer Formula: $D = k\lambda/\beta\cos\theta$, where, D is average grain size, nm; λ is the wave length of X-ray, nm; β is the width of the peak at its half height, degree; θ is diffractive angle, degree; k is a constant, 0.89.

The Seebeck coefficient and resistivity of the deposited films were measured by the Seebeck coefficient measurement system (TJU-EC2001) and the four-probe resistivity measuring device (TJU-EC2002) developed by Tianjin University at 25 ± 1 °C. The temperature difference for Seebeck coefficient measurement was controlled within 5 °C.

3. Electrodeposition process analysis

Cyclic voltammograms (CV) of Au electrode in Bi–Te–Se solution and Bi–Te–Sb solution (Table 1) are shown in Fig. 1. Two reductive peaks (A and B) can be observed in Fig. 1a), while only one oxidation peak occurs during anodic scanning process, which indicates that a single phase is formed during the cathodic scanning process. Furthermore, pink deposits were firstly observed during the cathodic scanning process from the open-circuit potential to peak A, which subsequently converted to dark deposits with the potential scanning negatively from peaks A to B, revealing that the deposition of Bi_2Se_3 occurs at more positive potentials as reported in the literature [20]. According to this phenomenon and previous work [21–23], peak A can be considered to be related to the adsorption and reduction of H_2SeO_3, and peak B is related to the formation of $Bi_2Te_{3-y}Se_y$ by a reaction among reduced Se, $HTeO_2^+$ and Bi^{3+}. The reaction process for peak B can be considered to be as follows:

$$H_2SeO_{3(aq)} \rightarrow H_2SeO_{3(ads)} \quad (1)$$

$$H_2SeO_{3(ads)} + 4H^+ + 4e^- \rightarrow Se + 3H_2O \quad (2)$$

$$Se + 2Bi^{3+} + 6e^- \rightarrow Bi_2Se_3 \quad (3)$$

$$HTeO_2^+ \rightarrow (HTeO_2^+)_{ads} \quad (4)$$

$$(HTeO_2^+)_{ads} + 3H^+ + 4e^- \rightarrow Te + 2H_2O \quad (5)$$

$$3Te + 2Bi^{3+} + 6e^- \rightarrow Bi_2Te_3 \quad (6)$$

$$ySe + 2Bi^{3+} + (3-y)HTeO_2^+ + (9-3y)H^+ + (12-4y)e^- \rightarrow Bi_2Te_{3-y}Se_y + (6-2y)H_2O \quad (7)$$

Fig. 1b) shows the CV of the Au electrode in Bi–Te–Sb solution (Table 1). During the cathodic process, the curve shows three apparent reduction peaks located at −19 mV(A′), −110 mV (B′) and −263 mV (C), separately. Similarly, there are also four oxidation peaks stood on 130 mV (D), 294 mV (E), 472 mV (F) and 512 mV (G) in the anodic scanning process, which indicates that more than one phase is formed during the cathodic scanning process.

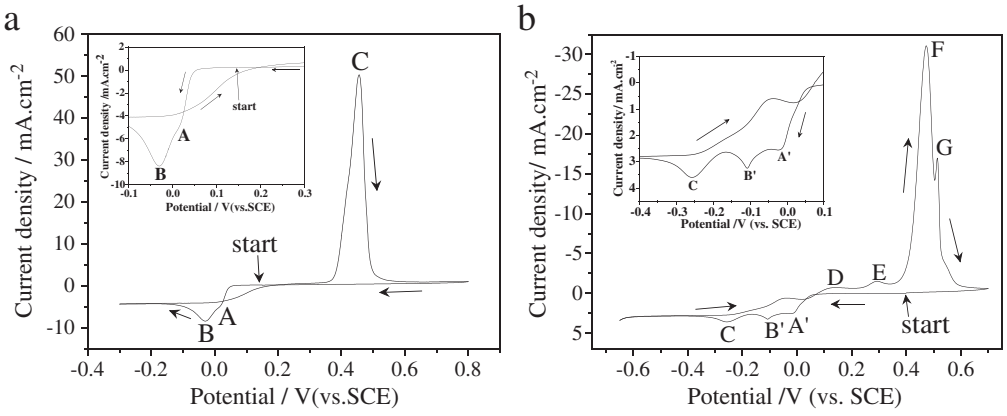

Fig. 1. Cyclic voltammograms of Au electrode in Bi–Te–Se a) and Bi–Te–Sb b) solutions; scanning rate = 10 mV/s, inset: partly amplified CVs.

Table 2
Composition of the films.

Specimen	Atomic percentage				Formula
	Bi	Te	Se	Sb	
Bi–Te–Se film	39.5	54.6	5.9	–	$Bi_{1.98}Te_{2.73}Se_{0.29}$
Bi–Te–Sb film	9.36	61.77	–	28.86	$Bi_{0.47}Sb_{1.44}Te_{3.09}$

Furthermore, it can be found that the reduction/oxidation process of the quaternary solution is irreversible on the surface of the Au electrode because of the obvious difference in the peak potentials and the peak shapes between the reduction peaks and oxidation peaks. On the other hand, gray deposits were firstly observed during the cathodic scanning process from the open-circuit potential to peak A′ on the Au electrodes and subsequently converted to dark ones when the scanning potential is more negative than peak B′. Our previous works [35–38] have shown that $HTeO^{2+}$ could adsorb strongly onto Au electrodes and the redox potential of reaction Sb^{III}/Sb is more negative than that of reaction $HTeO^{2+}/Te$ and Bi^{3+}/Bi. For this reason, the peak A′ at −19 mV presents the reduction of $HTeO^{2+}$ to Te^0, followed by the sequential reduction reaction of Bi^{3+} (peak B′) and Sb^{III} (peak C) to produce binary or ternary phases. The electrodeposition process of the Bi–Te–Sb solution could be described as follows:

$$HTeO_2^+ \rightarrow (HTeO_2^+)_{ads} \quad (8)$$

$$(HTeO_2^+)_{ads} + 3H^+ + 4e^- \rightarrow Te + 2H_2O \quad (9)$$

$$3Te + 2Bi^{3+} + 6e^- \rightarrow Bi_2Te_3 \quad (10)$$

$$(2-x)Bi^{3+} + xSbO^+ + yHTeO_2^+ + (2x+3y)H^+ + (6+4y)e^- \rightarrow Bi_{2-x}Sb_xTe_y + (x+2y)H_2O \quad (11)$$

$$3Te + 2SbO^+ + 4H^+ + 6e^- \rightarrow Sb_2Te_3 + 2H_2O \quad (12)$$

4. Composition, structure and morphology characterization of the electrodeposited n-type and p-type TE films

The compositions of the as-deposited films prepared in the two solutions (Table 1) are presented in Table 2. The results indicate that elements Bi, Te and Se have co-deposited from the Bi–Te–Se solution to form a film with a composition of $Bi_{1.98}Te_{2.73}Se_{0.29}$, and the similar process has also happened in the Bi–Te–Sb solution and the composition of the deposited film was $Bi_{0.47}Sb_{1.44}Te_{3.09}$.

The XRD spectra of the as-deposited and annealed Bi–Te–Se film and Bi–Te–Sb film are shown in Fig. 2. Both of the as-deposited films possess amorphous structure and their structure transfers gradually to crystal after anneal. The peaks in Fig. 2a) and b) are consistent very well with the standard powder XRD patterns of $Bi_2Te_{2.7}Se_{0.3}$(JCPDS 50-0954) and $Bi_{0.5}Sb_{1.5}Te_3$ (PDF49-1713), separately, revealing that the $Bi_2Te_{2.7}Se_{0.3}$ and $Bi_{0.5}Sb_{1.5}Te_3$ compounds can be synthesized by electrodeposition combining annealing treatment. The grain sizes of the annealed sample calculated by peak (0 1 5) in the XRD patterns are 36 nm and 48 nm for Bi–Te–Se film and Bi–Te–Sb films, separately, which mean that nano-crystalline films were formed after annealing treatment. Comparing the relative peak intensity of the annealed films (Table 3), it can be found that both the annealed films show a preferential orientation along the (0 1 5) crystalline plane, and the extent of the preferential orientation for the n-type Bi–Te–Se film is stronger than that for the p-type Bi–Te–Sb film.

The surface morphologies of as-deposited Bi–Te–Se and Bi–Te–Sb films prepared in the solutions (Table 1) are shown in Fig. 3. It can be seen that both of the films are dense and smooth, and n-type Bi–Te–Se film possesses smoother surface morphology than that of p-type Bi–Te–Sb film.

5. Performance of the deposited films

The performances of as-deposited and annealed films prepared in Bi–Te–Sb and Bi–Te–Sb solutions (Table 1), in terms of the Seebeck coefficients (S) and resistivities (ρ), are shown in Table 4. It can be seen that the Seebeck coefficient and the resistivity of p-type Bi–Te–Sb film are all decreased after anneal treatment. The value of the Seebeck coefficient decreases from 145 μV/K to 126 μV/K. However, the electrical resistivity of the as-deposited film is $7.22\times10^{-5}\,\Omega\,m$, and it reaches $2.45\times10^{-5}\,\Omega\,m$ after annealing treatment, being approximately 3 times lower than that of the as-deposited one. In other words, the decrease of the electrical resistivity is much more significant than that of the Seebeck coefficient, which indicates that the anneal treatment could improve the thermoelectric properties of electrodeposited p-type Bi–Te–Sb film efficiently. The effect of anneal treatment on the performances of n-type Bi–Te–Se film is different from that of p-type Bi–Te–Sb film. The anneal treatment cannot only decrease the resistivity remarkably, but also increases the Seebeck coefficient numbers for n-type Bi–Te–Se film.

Comparing with as-deposited n-type Bi–Te–Se film, the higher resistivity for as-deposited p-type Bi–Te–Sb film can be considered to be the major reason causing the coarser surface (Fig. 3). It can be considered that the thermal treatment altered the structure of the as-deposited n-type Bi–Te–Se film from the irregular amorphous state to more regular crystals as compound $Bi_2Te_{2.7}Se_{0.3}$, which leads to a lower electrical resistivity and higher Seebeck coefficient.

6. Proposed module of micro-thermoelectric power generator

We proposed an MTEG module in 2007 [34], which possesses a multilayer structure. It is an aggregation composed of a number of

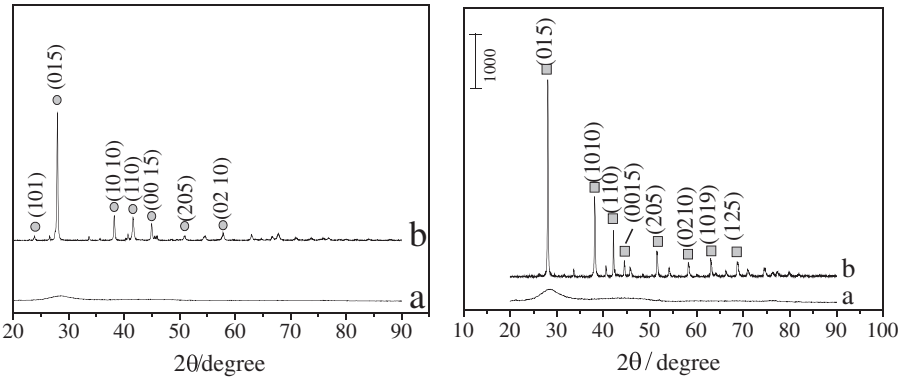

Fig. 2. XRD patterns of as-deposited and annealed Bi–Te–Se film a) and Bi–Te–Sb film b).● $Bi_2Te_{2.7}Se_{0.3}$ (JCPDS 50-0954), ■ $Bi_{0.5}Sb_{1.5}Te_3$ (PDF49-1713).

Table 3
Relative peak intensity (I/I_{max}) for annealed films calculated from Fig. 2.

(*h k l*)		(0 1 5)	(1 0 10)	(1 1 0)	(0 0 15)	(2 0 5)	(0 2 10)
Bi–Te–Sb film	Annealed films (I/I_{max})/%	100	56.3	27.6	12.7	15.4	10.6
	Powder XRD pattern (I/I_{max})/%	100	55	32	21	14	9
Bi–Te–Se film	Annealed films (I/I_{max})/%	100	19.4	17.3	13.1	3.4	5.9
	Powder XRD pattern (I/I_{max})/%	100	48.0	36.0	13.0	20.0	15.0

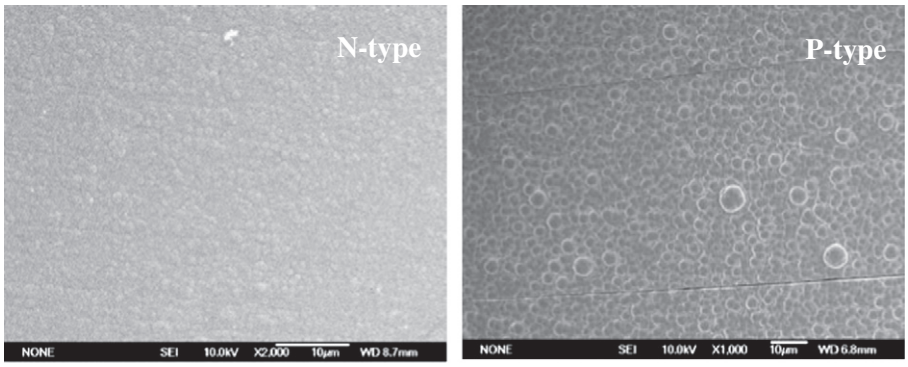

Fig. 3. SEM photos of electrodeposited n-type Bi–Te–Se and p-type Bi–Te–Sb films.

film-like thermoelectric components. The structure of the film-like thermoelectric components is shown in Fig. 4. Its structure includes an electric connecting layer, a left pole, a right pole, a p-type leg, an n-type leg and an insulating layer. There are two adjacent insulating layers, the one located at the bottom acts as the support of p-type legs and n-type legs while the upper one is used to form the micro-zones in which the p-type legs and n-type legs are electrodeposited. The p-type legs and n-type legs are electrically connected in series one by one using an electric connecting layer.

To get a high packing density of the thermocouples, an aggregative structure is designed and shown in Fig. 5. It can be found that a number of film-like thermoelectric components are aggregated together to form a multilayer structure, in which every two adjacent film-like thermoelectric components are electrically connected in series at the end of the poles by the pole connecting layer and the film-like thermoelectric components are bonded by the insulating connection layer. The multilayer structure ensures a much higher packing density of the thermocouples. It can also be found in the module that heat transfers along the surface direction of film TE legs. The length of the n-type legs and p-type legs is usually in millimeter range. This means that a higher temperature difference can be set up in this module.

An outer encapsulating layer is set up first on the outer-surface of the thermoelectric aggregation, and then a positive electrode and a negative electrode are set up separately on the outer-surface of the outer encapsulating layer as shown in Fig. 6. The positive electrode and the negative electrode are connected separately with the poles located separately at the two sides of the thermoelectric aggregation, and external load can be connected to the MTEG through the two electrodes.

Table 4
Performances of the deposited films.

Performance		Seebeck coefficient ($\mu V\,K^{-1}$)	Resistivity ($\Omega\,m$)	Power factor (mW/K^2m)
Bi–Te–Sb film	As-deposited	145	7.22×10^{-5}	0.22
	Annealed	126	2.45×10^{-5}	0.65
Bi–Te–Se film	As-deposited	−83.2	3.31×10^{-5}	0.21
	Annealed	−154.3	1.71×10^{-5}	1.34

Two hard plates with good thermal conductivity, called hard top plate and hard bottom plate, are set up separately on the top and bottom of the encapsulated thermoelectric aggregation separately through two thermal conductive layers (Fig. 7), and the thermal flow will transfer through the two hard plates. The thermal conductive layer acts also as the bond of the two hard plates. The structures showed in Fig. 7 are the appearance of the proposed MTEG module.

7. Fabrication and performances of the micro-thermoelectric power generator

Based on the proposed MTEG module mentioned above, film-like thermoelectric components were fabricated separately on a metallic

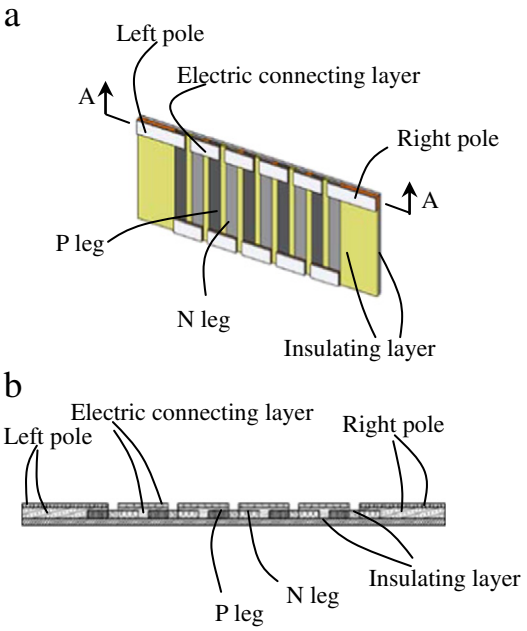

Fig. 4. Schematic view of the film-like thermoelectric component. a) Three-dimensional view; b) cross-sectional view along cross-section A.

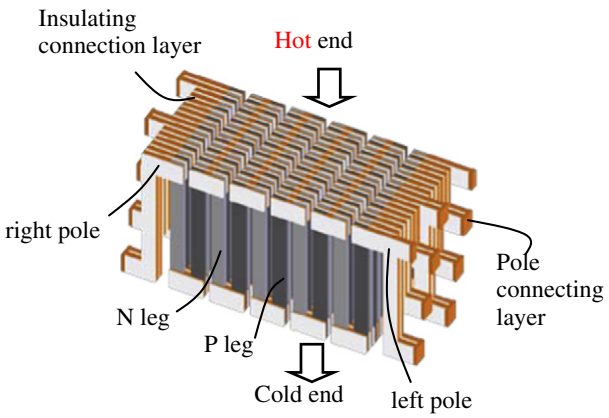

Fig. 5. Schematic view of the thermoelectric aggregation.

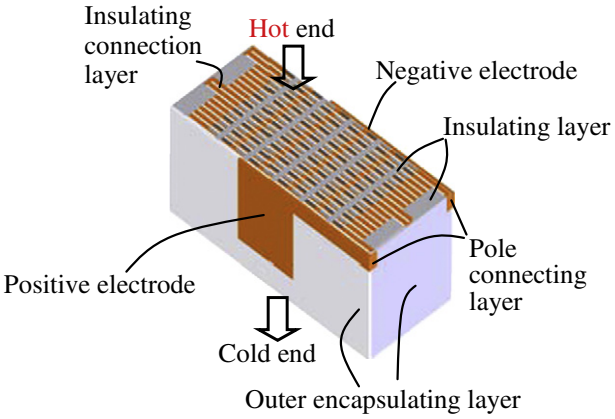

Fig. 6. Schematic view of the partly encapsulated thermoelectric aggregation.

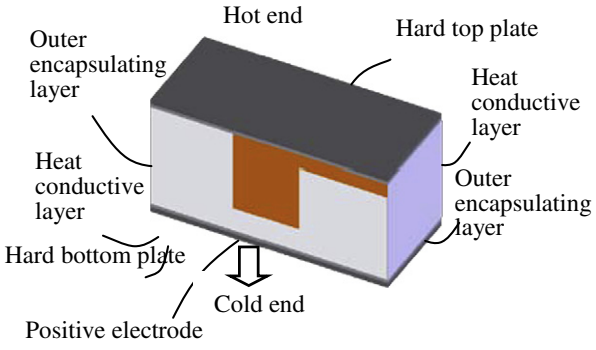

Fig. 7. Schematic appearance of the proposed MTEG module.

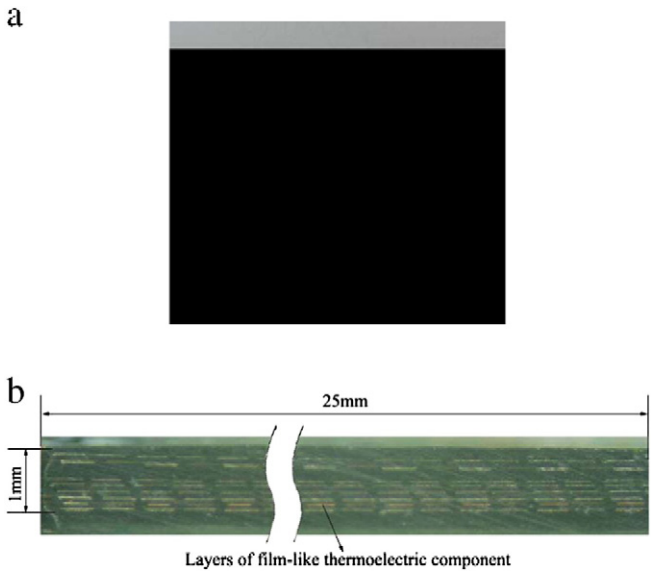

Fig. 9. Photos of the fabricated MTEG composed of eight film-like thermoelectric components a) and its cross-section b).

substrate by electrodepositing n-type legs (Bi–Te–Se film), p-type legs (Bi–Te–Sb film) and electric connecting layer (copper film) into the corresponding micro-zones which were prepared by photolithograph. Fig. 8 shows the fabricated film-like thermoelectric component composed of 20 p-type legs and 21 n-type legs. All the n-type legs and p-type legs possess the same size of 3.6 mm (length) × 0.4 mm (width) × 50 μm (thickness).

Thereafter, the fabricated film-like thermoelectric components were peeled from the metallic substrate and then bonded together layer by layer with epoxy resin to form a thermoelectric aggregation. Two silver wires acting as positive electrode and negative electrode were bonded separately onto the two sides of the fabricated thermoelectric aggregation with epoxy resin. Then an electroless plating copper process was conducted to connect every two adjacent film-like thermoelectric components and also the two silver wires with the fabricated thermoelectric aggregation electrically in series at the places of the pole connecting layer. Fig. 9a) is the photo of the MTEG fabricated in our lab, which contains eight layers of the film-like thermoelectric components (Fig. 9b) and 160 thermocouples. For easy holding, excess epoxy resin was covered around. The real size of the MTEG is 4 mm (height) × 25 mm (width) × 1 mm (thickness).

The internal resistance of the fabricated MTEG was measured to be 1.1 kΩ at room temperature. The output voltage and output power of the fabricated MTEG versus the current were also measured at 25 °C with a constant temperature difference $\Delta T = 20$ K and the results are shown in Fig. 10, the simulated curves are also shown in Fig. 10. With the increase of the current, the output power changes in a

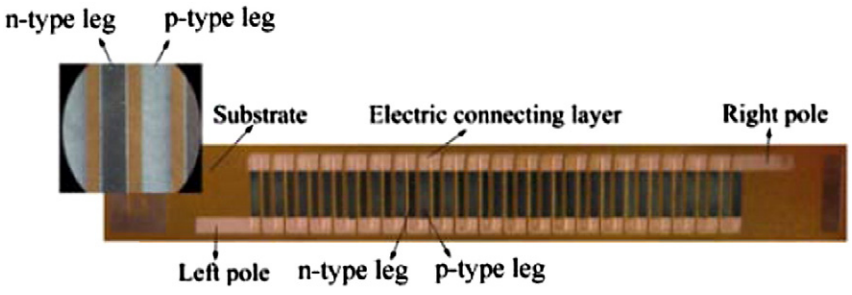

Fig. 8. Photo of the fabricated film-like thermoelectric component.

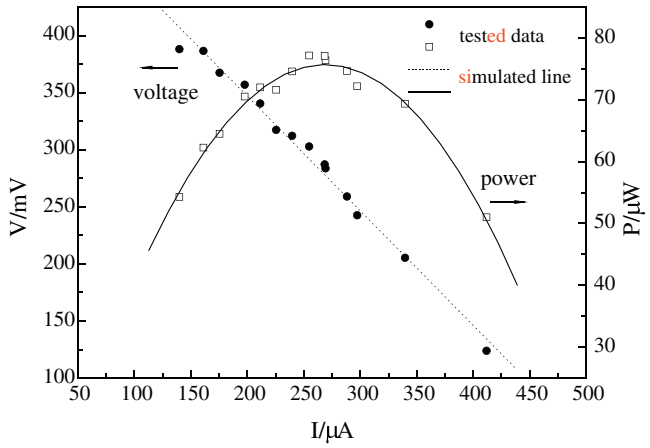

Fig. 10. Output voltage and power versus the current at 25 °C with a constant temperature difference ΔT = 20 K.

way like a mountain while the output voltage decreases constantly. The maximum output power is about 77 μW at current 268 μA, which corresponds to a maximum output power density of about 770 μW cm^{-3}. The open-circuit voltage of the fabricated MTEG was measured to be 660 mV at 25 °C with a constant temperature difference ΔT = 20 K.

A comparison between Whalen's MTEG and the author's MTEG is given in Table 5. It can be found that the volume of the author's MTEG with 160 TE couples is only 0.1 cm^3 while the volume of Whalen's MTEG with 11 TE couples is 4.3 cm^3. This reveals that numerous electrodeposited TE legs can be easily integrated into a small volume to form a thermoelectric pile, which is beneficial to the usage of the heat transferred through the MTEG more efficiently and brings a higher output power density at similar operating conditions. On the other hand, the internal resistance of the MTEG fabricated by electrodeposited film materials (~50 μm thickness) is much higher than that fabricated by wafers (215 μm thickness) cut from metallurgical ingot and the high internal resistance of the films results low current. The significant difference on the thickness of TE legs between the wafers (215 μm) and the electrodeposited films(~50 μm) is the major reason for the high internal resistance. The resistivity of the electrodeposited film materials can also be decreased farther by optimizing the preparation technology. For a practical application of MTEG, a lower internal resistance is necessary, which depends on a reasonable design of TE module and the improvement of material performance.

8. Conclusion

N-type $Bi_2Te_{2.7}Se_{0.3}$ compound and p-type $Bi_{0.5}Sb_{1.5}Te_3$ compound can be synthesized by electrodeposition combining annealing treatment. The as-deposited films possess amorphous structure and they can be transferred to nano-crystal after anneal treatment. The annealed films show a preferred orientation along the (015) crystal plane. Annealing treatment can also improve the performance of the electrodeposited films efficiently.

An MTEG module based on film thermoelectric materials has been proposed. The module possesses a multilayer structure, in which a number of film-like thermoelectric components are electrically connected in series. The remarkable characteristics of the proposed module are its high packing density of thermocouples and its heat transferring direction along the surface of the TE legs, which are beneficial to get higher output voltage and output power.

Based on the proposed module, a micro-thermoelectric power generator composed of 160 thermocouples was fabricated. Its internal resistance, its open-circuit voltage, maximum output power and corresponding power density under the temperature difference of 20 K at 25 °C were measured to be 1.1 kΩ, 660 mV, 77 μW and 770 μW cm^{-3}, respectively.

Acknowledgments

This work was co-supported by the International Cooperation Project of the Chinese Science and Technology Ministry (2009DFA62700) and the Doctorial Foundation Project of Chinese Education Ministry (200800560002).

References

[1] B.C. Sales, Science 295 (2002) 1248.
[2] W.S. Capinski, H.J. Maris, T. Ruf, M. Cardona, K. Ploog, D.S. Katzer, Phys. Rev. B 59 (1999) 8105.
[3] M.S. Dresselhaus, Y.M. Lin, G. Dresselhaus, X. Sun, Z. Zhang, S.B. CroAun, T. Koga, J.Y. Ying, The Eighteenth International Conference on Thermoelectrics, Baltimore, MD, U.S.A., 1999, p. 92.
[4] L.D. Hicks, M.S. Dresselhaus, Phys. Rev. B 47 (1993) 16631.
[5] L.D. Hicks, T.C. Harman, X. Sun, M.S. Dresselhaus, Phys. Rev. B 53 (1996) 10493.
[6] G.D. Mahan, H.B. Lyon, J. Appl. Phys. 76 (1994) 1899.
[7] R. Venkatasubramanian, E. Siivola, T. Colpitts, B. O'Quinn, Nature 413 (2001) 597.
[8] T.C. Harman, P.J. Taylor, D.L. Spears, M.P. Walsh, J. Electron. Mater. 29 (2000) L1.
[9] D.Y. Li, Y. Wu, R. Fan, P.D. Yang, A. Majumdar, Appl. Phys. Lett. 83 (2003) 3186.
[10] Y.D. Li, J.W. Wang, Z.X. Deng, Y.Y. Wu, X.M. Sun, D.P. Yu, P.D. Yang, J. Am. Chem. Soc. 123 (2001) 9904.
[11] C.J. Xiao, J.Y. Yang, W. Zhu, J.Y. Peng, J.S. Zhang, Electrochim. Acta 54 (2009) 6821.
[12] A.L. Prieto, R. Gronsky, T. Sands, A.M. Stacy, J. Electrochem. Soc. 149 (2002) C546.
[13] P. Heo, K. Hagiwara, R. Ichino, M. Okidob, J. Electrochem. Soc. 153 (2006) C213.
[14] X.H. Li, B. Zhou, L. Pu, J.J. Zhu, Cryst. Growth Des. 8 (2008) 771.
[15] D.D. Frari, S. Diliberto, N. Stein, C. Boulanger, J.M. Lecuire, Thin Solid Films 483 (2005) 44.
[16] B.Y. Yoo, C.K. Huang, J.R. Limb, J. Herman, M.A. Ryanb, J.P. Fleurial, N.V. Myung, Electrochim. Acta 50 (2005) 4371.
[17] E.J. Menke, M.A. Brown, Q. Li, J.C. Hemminger, R.M. Penner, Langmuir 22 (2006) 10564.
[18] S. Li, M.S. Toprak, H.M.A. Soliman, J. Zhou, M. Muhammed, D. Platzek, E. Muller, Chem. Mater. 18 (2006) 3627.
[19] L.X. Bu, W. Wang, H. Wang, Appl. Surf. Sci. 253 (2007) 3360.
[20] M. Takahashi, M. Kojima, S. Sato, N. Ohnisi, A. Nishiwaki, K. Wakita, T. Miyuki, S. Ikeda, Y. Muramatsu, J. Appl. Phys. 96 (2004) 5582.
[21] F. Xiao, C. Hangarter, B. Yoo, Y. Rheem, K.-H. Lee, N.V. Myung, Electrochim. Acta 53 (2008) 8103.
[22] D.D. Frari, S. Diliberto, N. Stein, C. Boulanger, J.M. Lecuire, J. Appl. Electrochem. 36 (2006) 449.
[23] B.Y. Yoo, F. Xiao, K.N. Bozhilov, J. Herman, M.A. Ryan, N.V. Myung, Adv. Mater. 19 (2007) 296.
[24] K. Tittes, A. Bund, W. Plieth, A. Bentien, S. Paschen, M. Plötner, H. Gräfe, W.J. Fischer, J. Solid State Electrochem. 7 (2003) 714.
[25] M. Takashiri, T. Shirakawa, K. Miyazaki, H. Tsukamoto, Sens. Actuators, A 138 (2007) 329.
[26] A. Yadav, K.P. Pipe, M. Shtein, J. Power Sources 175 (2008) 909.
[27] S.A. Whalen, C.A. Apblett, T.L. Aselage, J. Power Sources 180 (2008) 657.
[28] W. Glatz, S. Muntwyler, C. Hierold, Sens. Actuators, A 132 (2006) 337.
[29] G.J. Snyder, J.R. Lim, C.K. Huang, J.P. Fleurial, Nat. Mater. 2 (2003) 528.

Table 5
Comparison of the MTEGs fabricated by Whalen and author.

MTEGs	Numbers of the TE couples	Volume	Current	Voltage	Maximum output power.	Maximum output power density	Open-circuit voltage	Internal resistance
Whalen's	11	4.3 cm^3	11 mA	41 mV	450 μW	104 μW/cm^3	82 mV	3.7 Ω
Author's	160	0.1 cm^3	268 μA	287 mV	77 μW	770 μW/cm^3	660 mV	1.1 kΩ

Note: The current and voltage are corresponding to the maximum output power. The internal resistances were measured at room temperature. The open-circuit voltage, current and voltage of Whalen's MTEG were measured at room temperature with a constant temperature difference of 15 K, while that of the author's MTEG was measured at room temperature with a constant temperature difference of 20 K.

[30] L.X. Bu, W. Wang, H. Wang, Appl. Surf. Sci. 253 (2007) 3360.
[31] F.H. Li, W. Wang, Appl. Surf. Sci. 255 (2009) 4225.
[32] G.J. Snyder, J.R. Lim, C.K. Huang, J.P. Fleurial, Nature 2 (2003) 528.
[33] S.A. Whalen, C.A. Apblett, T.L. Aselage, J. Power Sources 180 (2008) 657.
[34] W. Wang, F.H. Li, Chinese invention patent, Patent No. 200710057345.0, (2007).
[35] Y.T. Jin, W. Wang, J. Electron. Mater. 39 (2010) 1469.
[36] F.H. Li, W. Wang, J. Appl. Electrochem. 40 (2010) 2005.
[37] F.H. Li, W. Wang, Electrochim. Acta 55 (2010) 5000.
[38] F.H. Li, W. Wang, J.P. Gao, J. Electron. Mater. 39 (2010) 1562.